Extended Nested Array with a Filled Sensor for DOA Estimation of Non-circular Signals

LI Xiaolong[1,2], *ZHANG Xiaofei*[1,2*], *SHEN Zihan*[1,2]

1. College of Electronic and Information Engineering, Nanjing University of Aeronautics and Astronautics, Nanjing 211106, P. R. China;

2. Key Laboratory of Dynamic Cognitive System of Electromagnetic Spectrum Space, Ministry of Industry and Information Technology, Nanjing University of Aeronautics and Astronautics, Nanjing 211106, P. R. China

(Received 25 September 2024; revised 31 December 2024; accepted 10 February 2025)

Abstract: Sparse array design has significant implications for improving the accuracy of direction of arrival (DOA) estimation of non-circular (NC) signals. We propose an extended nested array with a filled sensor (ENAFS) based on the hole-filling strategy. Specifically, we first introduce the improved nested array (INA) and prove its properties. Subsequently, we extend the sum-difference coarray (SDCA) by adding an additional sensor to fill the holes. Thus the larger uniform degrees of freedom (uDOFs) and virtual array aperture (VAA) can be abtained, and the ENAFS is designed. Finally, the simulation results are given to verify the superiority of the proposed ENAFS in terms of DOF, mutual coupling and estimation performance.

Key words: non-circular signal; extended nested array; sparse array; direction of arrival (DOA) estimation; sum-difference coarray

CLC number: TN925 **Document code:** A **Article ID:** 1005-1120(2025)01-0090-11

0 Introduction

Direction of arrival (DOA) estimation is a significant research field in array signal processing and is extensively applied to wireless communications, radar, and acoustic[1-9]. Many classical DOA estimation algorithms, such as MUSIC[10] and ESPRIT[11], are based on uniform linear arrays (ULAs). In order to avoid spatial aliasing, for a ULA, the spacing of neighboring sensors cannot exceed a half wavelength. And the estimable sources will not be more than the number of array elements, which means that at most K-1 signals can be detected by K sensors. Consequently, it is necessary to keep adding sensors in order to obtain larger aperture and degrees of freedom (DOFs).

In order to solve the problems of ULAs, various sparse arrays have been proposed, such as coprime arrays[12], nested arrays (NAs)[13], and so on[14-17]. Difference coarray (DCA) can be obtained to improve the estimation accuracy by virtualizing the sparse array. In order to further extend the virtual array aperture (VAA) and DOF, multiple improved structures have been proposed. The sensors in a subarray is doubled[18] to obtain the augmented coprime array (ACA). A new structure, the extended optimum coprime sensor array (EOCSA)[19], is proposed, which can achieve the same or even higher DOA estimation performance with fewer sensors. The redundant sensors are reduced[20], thus obtaining a thinned coprime array (TCA), which gives the larger VAA and DOFs for the same number of sensors compared to the ACA. However, the holes of coprime arrays after virtualization lead to a decrease in uniform DOFs (uDOFs).

DCA is hole-free in the traditional NSs, resulting in the larger uDOFs and the better estimated performance. However, it also has limitations, such

*Corresponding author, E-mail address: zhangxiaofei@nuaa.edu.cn.

How to cite this article: LI Xiaolong, ZHANG Xiaofei, SHEN Zihan. Extended nested array with a filled sensor for DOA estimation of non-circular signals[J]. Transactions of Nanjing University of Aeronautics and Astronautics, 2025,42(1):90-100.
http://dx.doi.org/10.16356/j.1005-1120.2025.01.007

as a large loss of DOFs caused by spatial smoothing, and mutual coupling between sensors. To solve these problems, super nested array (SNA) is proposed[21] to decrease mutual coupling by reducing the sensors at specific spacing. A coprime factor is introduced to expand the spacing of some elements, thus reducing the mutual coupling[22]. The augmented nested array (ANA)[23] disassembles the dense subarray and moves it to each side of the sparse subarray, which is able to increase the array aperture and DOF and decrease the effect of mutual coupling. The coprime array with displaced subarrays (CADiS)[24] introduces spacing between two coprime subarrays, which weakens the mutual coupling effect between the array elements and enhances the array aperture. But the holes in the DCA increase and therefore the consecutive DOF decreases. Based on the CADiS structure, a multi-layer filled coprime array (MLFCA) with hole-free coarray is proposed[25]. This array constructs a structure of multiple duplicated subarrays and fills the holes in the DCA, thus obtaining the extended DCA. These arrays extend the DCA by changing the position of the sensors, or adding new subarrays to fill holes in the original DCA. They all aim to extend the consecutive DCA so as to improve the DOA estimation accuracy for circular signals, but the enhancement is not obvious for non-circular (NC) signals. Compared with the current CADiS, ANA, and SNA, the array proposed in this paper not only extends the DCA, but also extends the sum coarray(SCA) for the properties of NC signals.

NC signals are important signal forms in modern communication systems which are widely used. Unlike circular signals, the covariance matrix and the pseudo-covariance matrix both can be utilized in DOA estimation, thus generating a larger virtual array. In order to improve the performance of DOA estimation of NC signals, many improved DOA estimation algorithms and sparse arrays have been proposed. The vectorized noncircular MUSIC(VNCM) algorithm[26] makes full use of DCA and SCA. This algorithm directly splices the consecutive parts of DCA and SCA to obtain SDCA. DsCAMpS[26] greatly increases the DOFs. NADiS[27] improves the nested array, which can obtain the extended sum difference coarray (SDCA). However, both DCA and SCA of this structure are not consecutive, and thus the VNCM algorithm cannot be used for DOA estimation.

In this paper, we aim to improve the DOA estimation accuracy of NC signals by sparse array design. The main idea is to get the larger uDOFs by adding an additional sensor to fill the holes in the SCA. Specifically, this array is obtained by two operations. Firstly, the improved nested array (INA) is proposed, which is composed of three subarrays. Its consecutive DCA is used to estimate the circular signal[28], but the SCA is not utilized. So in order to fully use the virtual array, an additional sensor is introduced to filling the holes to obtain a longer consecutive SDCA, thereby obtaining the extended nested array with a filled sensor (ENAFS). Compared with the conventional sparse arrays, the proposed ENAFS obtains increased uDOFs and enlarged VAA. And the mutual coupling effect is lower due to reducing the number of compact elements. The main work of this paper is summarized as follows:

(1) We introduce the INA structure and give the exact expression of the fillable holes in the SDCA.

(2) We propose an ENAFS structure by adding an additional sensor to fill the holes in the INA.

(3) We demonstrate the superiority of the proposed ENAFS in terms of DOF, mutual coupling and estimation performance through simulation and numerical analysis.

Notations: Lower-case bold characters indicate vectors (e.g., $\boldsymbol{a}$), upper-case bold characters indicate matrices (e.g., $\boldsymbol{A}$), and upper-case outlines denote sets (e.g., $\mathbb{V}$). $(\cdot)^{\mathrm{T}}$, $(\cdot)^{*}$ and $(\cdot)^{\mathrm{H}}$ stand for transpose, conjugation and conjugate transpose, respectively. $\langle a, b\rangle$ denotes a set of integers $\{z \in \mathbf{Z} \mid a \leqslant z \leqslant b\}$. $\otimes$ denotes the Kronecker product. $\odot$ denotes the Khatri-Rao(KR) product. vec is the vectorization operator.

1 Preliminaries

1.1 Received signal model

Assuming that there are K uncorrelated far-field signals incident from $\theta_1, \theta_2, \cdots, \theta_K$ to an array with N array elements, here N is the total number of elements; and the element position is $\tilde{\mathbb{L}} = d_0\mathbb{L} = d_0\{l_1, l_2, \cdots, l_N\}$, here $d_0 = \lambda/2$ and λ is the signal wavelength. The received signal can be expressed as

$$\boldsymbol{x}(t) = \boldsymbol{A}\boldsymbol{s}(t) + \boldsymbol{n}(t) \tag{1}$$

where $\boldsymbol{n}(t)$ is the additive white Gaussian noise with mean 0 and variance σ_n^2, $\boldsymbol{s}(t)$ the signal vector, $\boldsymbol{A} = [\boldsymbol{a}(\theta_1), \boldsymbol{a}(\theta_2), \cdots, \boldsymbol{a}(\theta_K)] \in \mathbf{C}^{N\times K}$ the direction matrix, and its kth direction vector is

$$\boldsymbol{a}(\theta_k) = [\mathrm{e}^{-\mathrm{j}2\pi l_1 d_0 \sin\theta_k/\lambda}, \mathrm{e}^{-\mathrm{j}2\pi l_2 d_0 \sin\theta_k/\lambda}, \cdots, \mathrm{e}^{-\mathrm{j}2\pi l_N d_0 \sin\theta_k/\lambda}]^{\mathrm{T}} \tag{2}$$

We assume that the signals are strictly non-circular, then the received signal vector $\boldsymbol{s}(t) = [s_1(t), s_2(t), \cdots, s_K(t)]^{\mathrm{T}}$ can be represented as

$$\boldsymbol{s}(t) = \boldsymbol{\Phi}\boldsymbol{s}_{\mathrm{R}}(t) \tag{3}$$

where $\boldsymbol{s}_{\mathrm{R}}(t)$ is the real-valued signal, $\boldsymbol{\Phi} = \mathrm{diag}\{\mathrm{e}^{-\mathrm{j}\varphi_1}, \mathrm{e}^{-\mathrm{j}\varphi_2}, \cdots, \mathrm{e}^{-\mathrm{j}\varphi_K}\}$ and the non-circular phase of the kth signal is denoted as φ_k. We also assume that all signals can be regarded as quasi-stationary processes[29].

Combining the received signal and its conjugate, we can get the extended received signal as[30]

$$\boldsymbol{x}_{\mathrm{e}}(t) = \begin{bmatrix} \boldsymbol{x}(t) \\ \boldsymbol{x}^*(t) \end{bmatrix} = \begin{bmatrix} \boldsymbol{A}\boldsymbol{\Phi} \\ \boldsymbol{A}^*\boldsymbol{\Phi}^* \end{bmatrix} \boldsymbol{s}_{\mathrm{R}}(t) + \begin{bmatrix} \boldsymbol{n}(t) \\ \boldsymbol{n}^*(t) \end{bmatrix} = \boldsymbol{A}_{\mathrm{e}}\boldsymbol{s}_{\mathrm{R}}(t) + \boldsymbol{n}_{\mathrm{e}}(t) \tag{4}$$

where $\boldsymbol{A}_{\mathrm{e}} = [(\boldsymbol{A}\boldsymbol{\Phi})^{\mathrm{T}}, (\boldsymbol{A}\boldsymbol{\Phi})^{\mathrm{H}}]^{\mathrm{T}}$ is the expanded direction matrix, and $\boldsymbol{n}_{\mathrm{e}}(t) = [\boldsymbol{n}^{\mathrm{T}}(t), \boldsymbol{n}^{\mathrm{H}}(t)]^{\mathrm{T}}$ the extended noise matrix.

In the fth time frame, here $f \in \langle 1, F\rangle$ and F is the total number of time frame, the covariance matrix of the extended received signal is denoted as

$$\boldsymbol{R}_{fx} = E[\boldsymbol{x}_{\mathrm{e}}(t)\boldsymbol{x}_{\mathrm{e}}^{\mathrm{H}}(t)] = \boldsymbol{A}_{\mathrm{e}}\boldsymbol{R}_{fs}\boldsymbol{A}_{\mathrm{e}}^{\mathrm{H}} + \sigma_n^2\boldsymbol{I}_{2N} \tag{5}$$

where $\boldsymbol{R}_{fs} = E[\boldsymbol{s}_{\mathrm{R}}(t)\boldsymbol{s}_{\mathrm{R}}^{\mathrm{H}}(t)] = \mathrm{diag}[\sigma_{f1}^2, \sigma_{f2}^2, \cdots, \sigma_{fK}^2]$ is the covariance matrix of the fth frame.

In order to obtain the received signal of the virtual SDCA, we vectorize the covariance matrix $\boldsymbol{R}_{fx}$, shown as

$$y_{f0} = \mathrm{vec}(\boldsymbol{R}_{fx}) = (\boldsymbol{A}_{\mathrm{e}}^* \odot \boldsymbol{A}_{\mathrm{e}})\boldsymbol{\gamma}_f + \sigma_n^2\mathrm{vec}(\boldsymbol{I}_{2N}) \tag{6}$$

where $\boldsymbol{\gamma}_f = [\sigma_{f1}^2, \sigma_{f2}^2, \cdots, \sigma_{fK}^2]^{\mathrm{T}} \in \mathbf{C}^{K\times 1}$. And we define $\boldsymbol{B}_{\mathrm{e}} = \boldsymbol{J}_{\mathrm{e}}(\boldsymbol{A}_{\mathrm{e}}^* \odot \boldsymbol{A}_{\mathrm{e}})$[26]. The kth column of $\boldsymbol{B}_{\mathrm{e}}$ can be expressed as

$$\boldsymbol{b}_{\mathrm{e}}(\theta_k, \varphi_k) = \boldsymbol{J}_{\mathrm{e}}\left(\boldsymbol{a}_{\mathrm{e}}^*(\theta_k, \varphi_k) \otimes \boldsymbol{a}_{\mathrm{e}}(\theta_k, \varphi_k)\right) = \begin{bmatrix} \boldsymbol{a}^*(\theta_k) \otimes \boldsymbol{a}(\theta_k) \\ \boldsymbol{a}^*(\theta_k) \otimes \boldsymbol{a}^*(\theta_k)\mathrm{e}^{\mathrm{j}2\varphi_k} \\ \boldsymbol{a}(\theta_k) \otimes \boldsymbol{a}(\theta_k)\mathrm{e}^{-\mathrm{j}2\varphi_k} \\ \boldsymbol{a}(\theta_k) \otimes \boldsymbol{a}^*(\theta_k) \end{bmatrix} \tag{7}$$

where φ_k is the non-circular phase of the kth signal, $\boldsymbol{a}^*(\theta_k) \otimes \boldsymbol{a}(\theta_k)$ and $\boldsymbol{a}(\theta_k) \otimes \boldsymbol{a}^*(\theta_k)$ can be represented as $\mathrm{e}^{-\mathrm{j}2\pi(l_i - l_j)d_0\sin\theta_k/\lambda}$ ($l_i, l_j \in \mathbb{L}$). Thus they can be regarded as the direction vectors of the DCA. $\boldsymbol{a}^*(\theta_k) \otimes \boldsymbol{a}^*(\theta_k)$ and $\boldsymbol{a}(\theta_k) \otimes \boldsymbol{a}(\theta_k)$ can be represented as $\mathrm{e}^{-\mathrm{j}2\pi(-l_i - l_j)d_0\sin\theta_k/\lambda}$ and $\mathrm{e}^{-\mathrm{j}2\pi(l_i + l_j)d_0\sin\theta_k/\lambda}$ ($l_i, l_j \in \mathbb{L}$). Similarly, they can be regarded as the direction vectors of SCA.

By sorting $\boldsymbol{b}_{\mathrm{e}}(\theta_k, \varphi_k)$ in Eq.(7) according to the positions of the array elements, we can obtain the direction vector of the SDCA, shown as

$$\boldsymbol{b}(\theta_k, \varphi_k) = \begin{bmatrix} \boldsymbol{b}_{\mathrm{s}}^-(\theta_k)\mathrm{e}^{\mathrm{j}2\varphi_k} \\ \boldsymbol{b}_{\mathrm{d}}(\theta_k) \\ \boldsymbol{b}_{\mathrm{s}}^+(\theta_k)\mathrm{e}^{-\mathrm{j}2\varphi_k} \end{bmatrix} = \boldsymbol{\Theta}(\theta_k)\boldsymbol{\varphi}(\varphi_k) \tag{8}$$

where $\boldsymbol{\Theta}(\theta_k) = \mathrm{blkdiag}\{\boldsymbol{b}_{\mathrm{s}}^-(\theta_k), \boldsymbol{b}_{\mathrm{d}}(\theta_k), \boldsymbol{b}_{\mathrm{s}}^+(\theta_k)\}$, here blkdiag represents generating a block diagonal matrix, $\boldsymbol{b}_{\mathrm{s}}^-(\theta_k)$ and $\boldsymbol{b}_{\mathrm{s}}^+(\theta_k)$ represent the direction vectors of the SCA for the negative and positive axis, respectively, and $\boldsymbol{b}_{\mathrm{d}}(\theta_k)$ represents the direction vector of the DCA; $\boldsymbol{\varphi}(\varphi_k) = [\mathrm{e}^{\mathrm{j}2\varphi_k}, 1, \mathrm{e}^{-\mathrm{j}2\varphi_k}]^{\mathrm{T}}$.

By performing the same row operation on y_{f0}, we can obtain the equivalent received signal vector $\boldsymbol{y}_f \in \mathbf{C}^{(2R_3+1)\times 1}$ of the SDCA, shown as

$$\boldsymbol{y}_f = \boldsymbol{B}\boldsymbol{\gamma}_f + \boldsymbol{u} \tag{9}$$

where $\boldsymbol{B} = [\boldsymbol{b}(\theta_1, \varphi_1), \boldsymbol{b}(\theta_2, \varphi_2), \cdots, \boldsymbol{b}(\theta_K, \varphi_K)]$ is the direction matrix of the SDCA obtained by virtualization, and $\boldsymbol{u}$ the vector with all zeros except for 1 at the middle position. The equivalent received signal can be expressed as

$$\boldsymbol{Y} = \boldsymbol{B}\boldsymbol{\Gamma} + \boldsymbol{u}\boldsymbol{e}_F^{\mathrm{T}} \tag{10}$$

where $\boldsymbol{\Gamma} = [\boldsymbol{\gamma}_1, \boldsymbol{\gamma}_2, \cdots, \boldsymbol{\gamma}_F]$ and $\boldsymbol{e}_F = [1, 1, \cdots, 1]^{\mathrm{T}}$.

1.2 Reduced dimensional MUSIC

The matrix $\boldsymbol{\Theta}(\theta_k)$ in Eq.(8) contains only an-

gles and the vector $\boldsymbol{\varphi}(\varphi_k)$ contains only non-circular phases. It separates the DOA and non-circular phase in the direction vector. Therefore the reduced dimensional MUSIC algorithm can be used for DOA estimation[31]. The spectral function of RD-MUSIC algorithm is given by

$$P(\theta)=\boldsymbol{e}^{\mathrm{H}}\left(\boldsymbol{\Theta}^{\mathrm{H}}(\theta)\hat{\boldsymbol{E}}_{\mathrm{n}}\hat{\boldsymbol{E}}_{\mathrm{n}}^{\mathrm{H}}\boldsymbol{\Theta}(\theta)\right)^{-1}\boldsymbol{e} \tag{11}$$

where $\boldsymbol{e}=[0,1,0]^{\mathrm{T}}$ and $\hat{\boldsymbol{E}}_{\mathrm{n}}$ represents the estimate of the noise subspace.

2 Extended NA with a Filled Sensor

2.1 Prototype NA

A prototype NA contains a dense subarray and a sparse subarray. Fig.1 shows the structure of a prototype NA with 10 array elements, where the adjacent numbers represent a physical spacing of half a wavelength. Fig.1(a) is the positions of physical array elements; Fig.1(b) is the DCA of the NA, which is continuously distributed in $[-R_1,R_1]=[-29,29]$; Fig.1(c) is the SCA, which is continuously distributed in $\pm[R_2,R_3]=\pm[2,36]$; and Fig.1(d) is the SDCA, continuously distributed in $[-R_3,R_3]=[-36,36]$. NA can be directly used for DOA estimation of NC signals. However, the overlap between DCA and SCA can seriously reduce the uDOFs, resulting in a decrease in the DOA estimation accuracy.

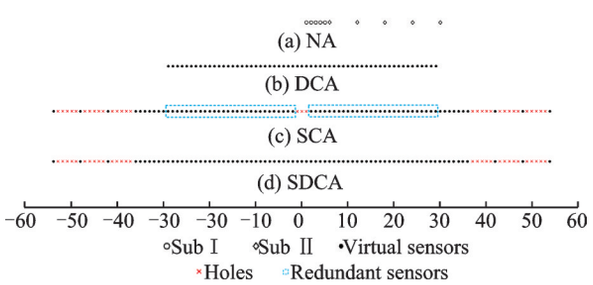

Fig.1 Structure of the prototype NA ($N=10$)

2.2 Extended NA based on hole representation and filling strategy

In order to increase the uDOFs and reduce the redundancy between DCA and SCA, an extended NA with a filled sensor, termed ENAFS, is designed in this subsection.

Definition Assume that $N_1\geqslant 1$ and $N_2\geqslant 2$, the proposed ENAFS is defined by

$$\begin{cases}\mathbb{S}_{\mathrm{ENAFS}}=(\mathbb{S}_1\cup\mathbb{S}_2\cup\mathbb{S}_3\cup\mathbb{S}_4)d\\ \mathbb{S}_1=0\\ \mathbb{S}_2=N_1+\langle 0,N_2-1\rangle(N_1+2)\\ \mathbb{S}_3=(N_1N_2+2N_2-1)+(\langle 0,N_1-2\rangle,N_1)\\ \mathbb{S}_4=\begin{cases}N_1N_2+2N_1 & N\text{ is even}\\ N_1N_2+2N_1-2 & N\text{ is odd}\end{cases}\end{cases} \tag{12}$$

where $d=\lambda/2$; $\mathbb{S}_1$, $\mathbb{S}_2$, $\mathbb{S}_3$ and $\mathbb{S}_4$ represent the four subarrays, respectively. The optimal choices of subarray parameters can be expressed as follows.

(1) When the total number N is odd, $N_1=(N-1)/2-1$, $N_2=(N-1)/2$.

(2) When the total number N is even, $N_1=N/2-2$, $N_2=N/2$.

Fig.2 illustrates the proposed ENAFS. For the proposed structure, the following properties hold for its virtual arrays.

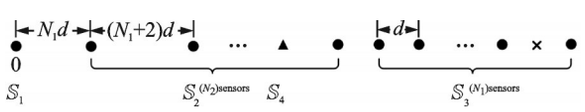

Fig.2 Array geometry of ENAFS

Property 1 The proposed ENAFS has the following properties.

(1) The DCA is continuous in the range $\langle -R_1,R_1\rangle$, where $R_1=N_1N_2+N_1+2N_2-3$.

(2) The SCA is continuous in the range $\pm\langle R_2,R_3\rangle$, where $R_2=N_1N_2+2N_2-2$, $R_3=2N_1N_2+2N_1+4N_2-4$.

(3) The SDCA is continuous in the range $\langle -R_3,R_3\rangle$ and the number of uDOFs is $4N_1N_2+4N_1+8N_2-7$.

Proof

(1) It is known that DCA is symmetric, so that the consecutive range $\langle -R_1,R_1\rangle$ can be equated to the range $\langle 0,R_1\rangle$. And 0 is always contained in the DCA, so it is enough to prove that it is consecutive in $\langle 1,R_1\rangle$.

$\mathbb{S}_1$ is the sensor located at the origin, and its own DCA is

$$\mathrm{diff}(\mathbb{S}_1,\mathbb{S}_1)=\{\tilde{\rho}_i^1\}=\{0\} \tag{13}$$

$\mathbb{S}_2$ is a sparse subarray and its own DCA is denoted as

$$\mathrm{diff}(\mathbb{S}_2,\mathbb{S}_2)=\{\tilde{\rho}_i^2\}=\{(N_1+2)l_{2v}\}$$
$$1\leqslant i\leqslant N_2-1,\quad 1\leqslant l_{2v}\leqslant N_2-1 \tag{14}$$

$\mathbb{S}_3$ is a uniform subarray with N_1 sensors, and its own DCA is

$$\begin{aligned}\mathrm{diff}(\mathbb{S}_3,\mathbb{S}_3)&=\{\tilde{\rho}_i^3\}=\{l_{3v}\}\\ 1\leqslant i\leqslant N_1,\quad 1\leqslant l_{3v}\leqslant N_1\end{aligned}\tag{15}$$

For subarray 2 and subarray 3, the DCA between them can be expressed as

$$\begin{aligned}&\mathrm{diff}(\mathbb{S}_3,\mathbb{S}_2)=\{\tilde{\rho}_i^{32}\}=\{l_{3v}+[N_1+(N_1+2)l_{2v}]\}\\ &1\leqslant i\leqslant N_2N_1,\ 0\leqslant l_{2v}\leqslant N_2-1,0\leqslant l_{3v}\leqslant N_1-1\end{aligned}\tag{16}$$

By placing the three nested subarays, an INA can be assembled with a DCA that is consecutive in the range $\langle -R_1,R_1\rangle$. Combining Eqs.(13—16), for the INA consisting of $\mathbb{S}_1$, $\mathbb{S}_2$ and $\mathbb{S}_3$, the DCA is consecutive in the full range $[1,N_1N_2+N_1+2N_2-3]$. Therefore the item (1) of Property 1 is established.

(2) The same as the proof of the item (1), SCA is also symmetric. Thus it is only necessary to prove that it is consecutive in the range $\langle R_2,R_3\rangle$.

For the INA consisting of $\mathbb{S}_1$, $\mathbb{S}_2$ and $\mathbb{S}_3$, we can obtain their SCAs, shown as

$$\mathrm{sum}(\mathbb{S}_1,\mathbb{S}_1)=\{0\}\tag{17}$$

$$\begin{aligned}\mathrm{sum}(\mathbb{S}_2,\mathbb{S}_2)&=\{2N_1+(N_1+2)(l_{2v}+l_{2\omega})\}\\ &0\leqslant l_{2v},l_{2\omega}\leqslant N_2-1\end{aligned}\tag{18}$$

$$\begin{aligned}\mathrm{sum}(\mathbb{S}_3,\mathbb{S}_3)=\{&(2N_1N_2+4N_2-2)+\\ &(\langle 0,2N_1-2\rangle,2N_1)\}\end{aligned}\tag{19}$$

The sets of SCA between $\mathbb{S}_1$, $\mathbb{S}_2$ and $\mathbb{S}_3$ can be respectively denoted as

$$\begin{aligned}\mathrm{sum}(\mathbb{S}_2,\mathbb{S}_1)&=\{N_1+(N_1+2)l_{2v})\}\\ &0\leqslant l_{2v}\leqslant N_2-1\end{aligned}\tag{20}$$

$$\begin{aligned}\mathrm{sum}(\mathbb{S}_3,\mathbb{S}_1)=\{&(N_1N_2+2N_2-1)+\\ &(\langle 0,N_1-2\rangle,N_1)\}\end{aligned}\tag{21}$$

$$\begin{aligned}\mathrm{sum}(\mathbb{S}_3,\mathbb{S}_2)=\{&(N_1N_2+N_1+2N_2-1)+\\ &(N_1+2)l_{2v}+(\langle 0,N_1-2\rangle,N_1)\}\\ &0\leqslant l_{2v}\leqslant N_2-1\end{aligned}\tag{22}$$

Combining Eqs.(17—22), we can obtain that the first virtual element of the SCA is $R_2=N_1+(N_1+2)(N_2-1)=N_1N_2+2N_2-2$. And there are holes in the consecutive parts of the SCA due to the holes in $\mathbb{S}_3$, i.e.

$$H=\mathbb{H}_1+\mathbb{H}_2\tag{23}$$

$$\mathbb{H}_1=\begin{cases}N_1N_2+4N_1+\langle 0,N_1-1\rangle(N_1+2) & N\text{ is even}\\ N_1N_2+4N_1+2+\langle 0,N_1\rangle(N_1+2) & N\text{ is odd}\end{cases}\tag{24}$$

$$\mathbb{H}_2=-\mathbb{H}_1\tag{25}$$

Due to the symmetry of the positive and negative holes, we can obtain the complete set of holes from $\mathbb{H}_1$. When N is even, the starting position of the holes is $N_1N_2+4N_1$, and the spacing is N_1+2. It can be viewed as a virtual SCA of an additional sensor and $\mathbb{S}_2$. When N is odd, the starting position of the holes is $N_1N_2+4N_1+2$, and the spacing is N_1+2. It can also be viewed as a virtual SCA of an additional sensor and $\mathbb{S}_2$. Consequently, whether the total number is odd or even, the holes in the SCA can be filled by adding a certain element. In order to generate the increased SCA, we introduce an additional sensor, denoted as $\mathbb{S}_4$, to fill the holes in the SCA of the INA. The position of the additional sensor can be obtained by the following equation

$$\mathbb{S}_4=\mathbb{H}_1-\mathbb{S}_2'\tag{26}$$

where the number of $\mathbb{S}_2'$ is the same as $\mathbb{H}_1$. When N is even, $\mathbb{S}_2'$ takes the last N_1 elements of $\mathbb{S}_2$. When N is odd, $\mathbb{S}_2'$ takes the last N_1+1 elements of $\mathbb{S}_2$. According to Eq.(26), we can obtain the location of the additionaol sensor. Moreover, a consecutive SCA can be obtained by introducing the $\mathbb{S}_4$, and $R_3=2N_1N_2+2N_1+4N_2-4$.

$$\mathbb{S}_4=\begin{cases}N_1N_2+2N_1 & N\text{ is even}\\ N_1N_2+2N_1-2 & N\text{ is odd}\end{cases}\tag{27}$$

(3) Because $N_1\geqslant 1$, $R_1=N_1N_2+N_1+2N_2-3$, and $R_2=N_1N_2+2N_2-2$, we can derive that $R_1\geqslant R_2$ is always valid. Thus the SDCA is consecutive in the range $\langle -R_3,R_3\rangle$.

As an example, for the INA structure with nine array elements, the set of hole locations can be represented as $\mathbb{H}_1=\{29,34,39,44\}$, $\mathbb{H}_2=\{-29,-34,-39,-44\}=-\mathbb{H}_1$, and the additional sensor $\mathbb{S}_4=N_1N_2+2N_1=\{21\}$. Fig.3 shows the ENAFS structure. The total number is 10, and the consecutive part is $[-52,52]$. The ENAFS yields a larger

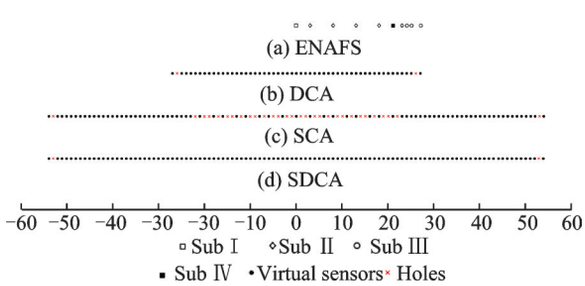

Fig.3 Coarrays of ENAFS($N=10$)

consecutive SDCA than the NA with the same number of sensors.

3 Performance Analysis

3.1 Coarray redundancy

The proposed ENAFS can reduce the redundancy between DCA and SCA and significantly increase the uDOFs. To present the advantages more clearly, we demonstrate the VAA, redundant virtual sensors, and DOF for different sparse arrays in Table 1. We also compare the redundancy of different sparse arrays in Fig.4. Redundancy ratio η is an important metric for judging the performance of an array, and it indicates the duplication of the virtual array elements. A small redundancy ratio indicates that most of the virtual arrays are utilized. We can see that because the SCA and DCA of NA and SNA 2[21] have many duplicate parts, the redundancy increases as array elements increases. In the DsCAMpS[26], both DCA and SCA have long consecutive segments, but there is repetition between the two, leading to a high redundancy. The ANA Ⅰ 1 and ANA Ⅱ 1 proposed in Ref.[17] have very low coarray redundancy, but the proposed structure is still superior to these arrays. Because the first subarray of the ENAFS has the large spacing of array elements and the second subarray has the smaller spacing of array elements, the SCA is more outwardly expanded, resulting in very small redundancy ratio.

Table 1 Comparison of properties for different sparse arrays

Array	Number of sensors	VAA	Redundant virtual sensors	DOF
DsCAMpS	$2N_1+P_2N_2-2$	$4P_2N_1N_2-4N_2$	$2(P_2-2)N_1N_2+4N_2+4N_1-2$	$\begin{cases}2(2P_2-1)N_1N_2+2N_2+2N_1-1 & N_1>N_2>2\\ 2(2P_2-1)N_1N_2+2N_1-1 & N_1>N_2=2\end{cases}$
ACA	$2N_1+N_2-1$	$8N_1N_2-4N_2$	$4N_1+2N_2-2$	$4N_1N_2+2N_1-1$
NA	N_1+N_2	$4N_1N_2+4N_2$	$2N_1N_2+2N_2-4$	$2N_1N_2+2N_1+2N_2+3$
ENAFS	N_1+N_2+2	$4N_1N_2+4N_1+8N_2-4$	$2N_1+4N_2-1$	$4N_1N_2+4N_1+8N_2-7$

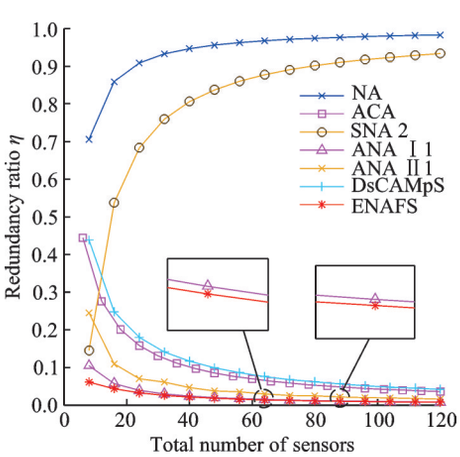

Fig.4 Redundancy ratio of different arrays

Table 2 Comparison of virtual array parameters for different arrays

Array	Array parameter	VAA	dDOF	sDOF	η/%	DOF
DsCAMpS	$M=3,N=4,P_2=3$	132	61	122	37.6	133
ANA Ⅰ1	$N_1=8,L_1=5$	272	135	30	6.5	155
ANA Ⅱ1	$L_1=2,L_2=2,N_2=4,d_{12}=6,d_{21}=5$	316	159	42	12.3	179
SNA 2	$N_1=7,N_2=8$	256	127	124	56.0	161
ACA	$M=5,N=6$	216	69	90	23.3	129
NA	$N_1=7,N_2=8$	256	127	142	85.5	145
ENAFS	$N_1=6,N_2=7$	244	119	134	5.0	241

3.2 DOF and VAA

Table 2 gives a comparison of main parameters of different array structures for N=15. Fig.5 and Fig.6 compare the DOF and VAA for different array structures. Due to its design targeting SDCA, NADiS[27] can achieve significantly larger DOF and VAA. Although the ENAFS does not have a clear advantage in VAA, due to its low redundancy, maximum DOFs can be obtained. And the DOF of NA is not satisfactory due to the large co-array redundancy. ANA can get a more prominent DOF of DCA (dDOF), but the DOF is also not as good as the proposed ENAFS because its DOF of SCA (sDOF) is limited.

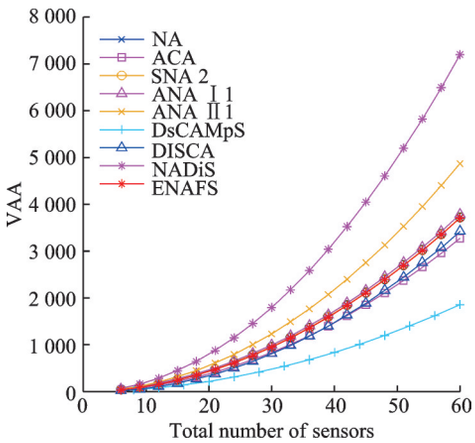

Fig.5 VAA of different sparse arrays

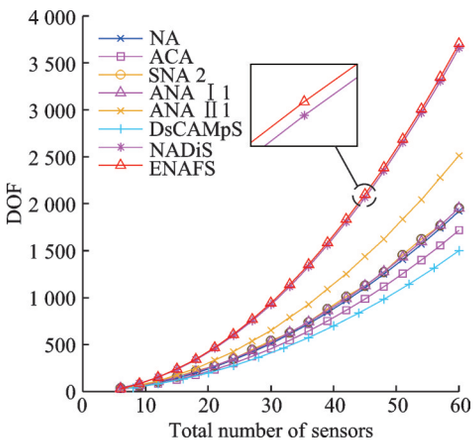

Fig.6 DOF of different sparse arrays

4 Simulation Results

In this section, we used the signal model and the RD-MUSIC algorithm introduced in Section 1 to evaluate the performance of the proposed ENAFS. We use the Monte-Carlo trials to compare the performance of different arrays. 500 experiments are performed for each comparison and the performance is evaluated using the root mean square error (RMSE), where RMSE is defined as

$$\mathrm{RMSE}=\sqrt{\frac{1}{500K}\sum_{n=1}^{500}\sum_{k=1}^{K}(\theta_k-\hat{\theta}_{k,n})^2} \tag{28}$$

where $\hat{\theta}_{k,n}$ represents the estimation of the kth signal in the nth trial.

4.1 Reduced dimensional MUSIC spectra

We show the reduced dimensional MUSIC spectra of several sparse arrays under the condition that $N=10$, where the red line represents the real DOA. Fig.7 depicts the MUSIC spectrum, where the number of sources $K=14$, the number of snapshots $J=500$, the signal-to-noise ratio SNR=0 dB and the absence of mutual coupling. Fig.8 shows the MUSIC spectra of different sparse arrays in the presence of mutual coupling, where $K=14$, $J=500$, SNR=0 dB and $c_1=0.25\mathrm{e}^{\mathrm{j}\pi/3}$[20,32-34].

All arrays can discriminate 14 sources with 10 array elements. However, due to various factors such as the number of uDOFs and array spacing, there is a gap in the performance between different arrays. The best MUSIC spectra is obtained for ENAFS in the presence and absence of mutual coupling, which is attributed to larger SDCA and sensors spacing.

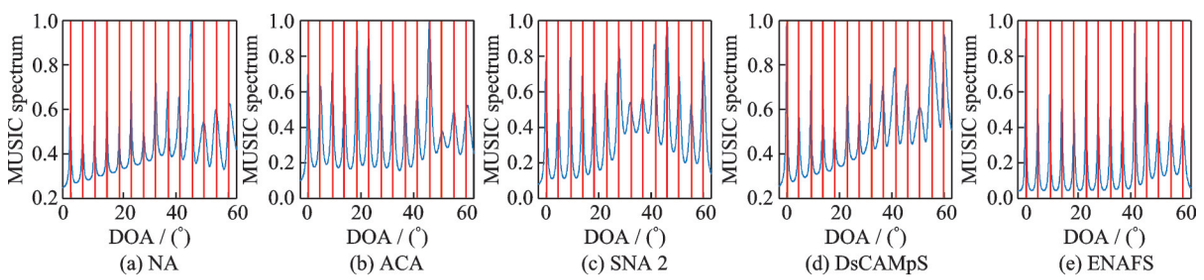

Fig.7 RD-MUSIC spectra without mutual coupling

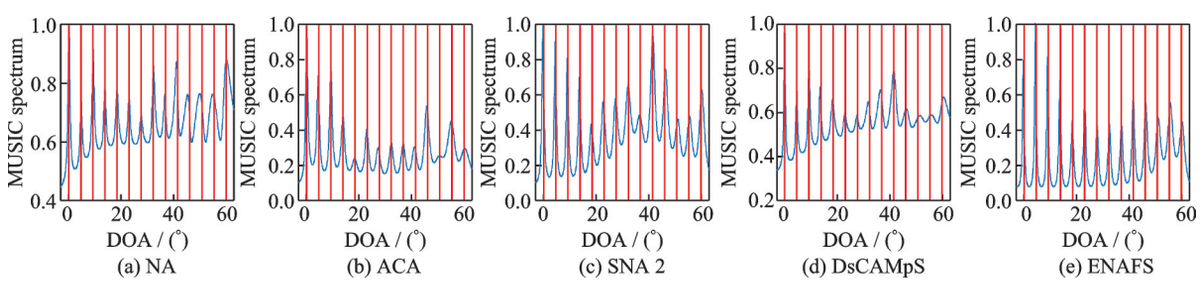

Fig.8 RD-MUSIC spectra with mutual coupling

4.2 Comparison of RMSE with different SNRs

In order to compare the performance under different SNRs, we performed simulations using RMSE as the evaluation criterion. Fig.9 depicts the comparison of RMSE of different sparse arrays in the absence of mutual coupling, where the number of snapshots $J=500$ and the number of sources $K=14$. As can be seen from Fig.9, in the absence of mutual coupling, the ENAFS has more accurate DOA estimation results than several other arrays due to having the longest SDCA.

Fig.10 illustrates the comparison of RMSE in the presence of mutual coupling, where $J=500$, $K=14$ and $c_1=0.15e^{j\pi/3}$. It can be seen that the ENAFS also gives better estimation performance in the presence of mutual coupling. The ENAFS performs significantly better than other arrays under low SNR. As the SNR increases, the gap gradually becomes small, but the advantage still exists. This is attributed to the large array element spacing and long SDCA.

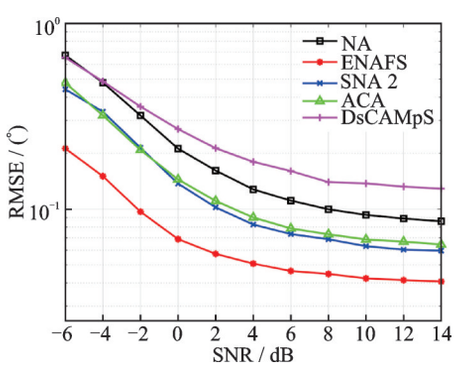

Fig.9 RMSE versus SNR for different arrays without mutual coupling($J=500$, $K=14$)

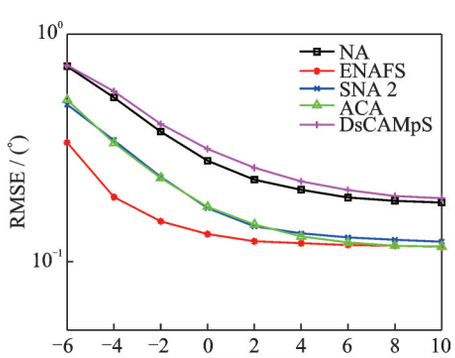

Fig.10 RMSE versus SNR for different arrays with mutual coupling($J=500$, $K=14$ and $c_1=0.15e^{j\pi/3}$)

4.3 Comparison of RMSE with different snapshots

The performance variation of RMSE with snapshot is an important factor in evaluating arrays. Fig.11 illustrates the change of RMSE with snapshots without mutual coupling, where SNR=5 dB and $K=14$. It can be seen that ENAFS produces a smaller RMSE, which is due to the larger SDCA. The RMSE order is the same as the SDCA size order, in the order of DsCAMpS, NA, ACA, SNA 2, and ENAFS. This suggests that a large SDCA can improve the estimation accuracy.

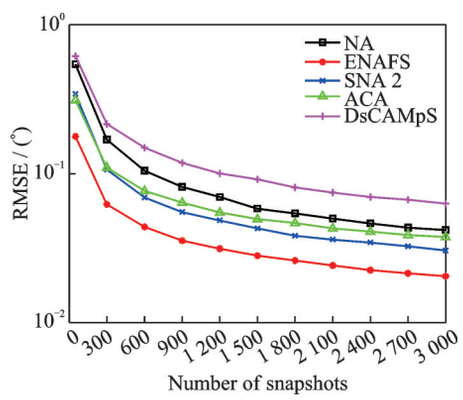

Fig.11 RMSE versus snapshots for different arrays without mutual coupling(SNR=5 dB, $K=14$)

4.4 Comparison of RMSE with different strengths of mutual coupling

The proposed ENAFS reduces the mutual coupling effect since it reduces the number of dense array elements. Fig.12 illustrates the change of RMSE with mutual coupling, where SNR = 0 dB, number of sources $K=12$ and $J=500$. The result shows that the RMSE of different arrays in-

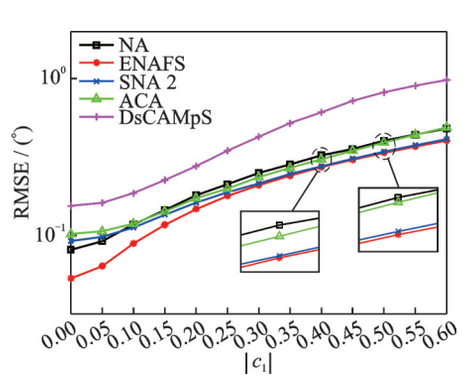

Fig.12 RMSE versus mutual coupling strengths for different arrays(SNR=5 dB, $J=500$ and $K=12$)

creases with the enhancement of mutual coupling. DsCAMpS has the largest RMSE because of its small uDOFs. ACA has a smaller RMSE than the NA because of its larger array element spacing. The proposed ENAFS has the minimum RMSE.

4.5 Comparison of resolution probability of different arrays

Fig.13 illustrates the resolution probability of different arrays for two closely located sources. We set the angle of the first source to be $\theta_1=30^\circ$, and the spacing between the two sources is set as

$$\boldsymbol{\Delta}=[0.2^\circ,0.3^\circ,0.45^\circ,0.6^\circ,0.75^\circ,0.9^\circ,1.05^\circ,1.2^\circ,1.35^\circ,1.5^\circ] \tag{29}$$

It can be seen from Fig.13 that when the source spacing is small, ACA and DsCAMpS have a small resolution probability. Due to the long consecutive SDCA of ENAFS, it can achieve angle estimation with very small source spacing. When the spacing between the two sources is just 0.45°, ENAFS can achieve an estimated success rate of 86.4%. When the source spacing is larger than 0.6°, ENAFS can achieve almost 100% resolution probability.

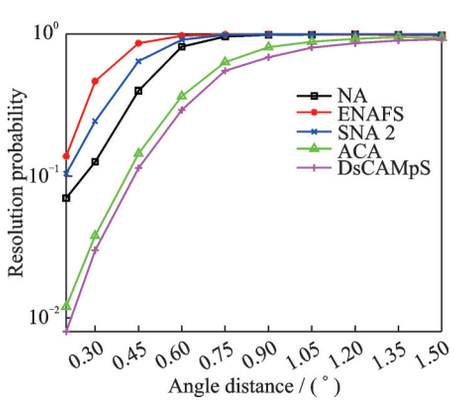

Fig.13 Resolution probability with two closely located sources of different arrays

5 Conclusions

We proposed an ENAFS array configuration for DOA estimation of NC signals. By analyzing the holes in the SCA of INA, we found that a longer consecutive SDCA could be obtained by introducing an additional sensor. We derived the locations of the holes and calculated the location of the additional sensor. Further, we designed the ENAFS by adding an additional sensor. The proposed ENAFS can obtain increased uDOFs, extended VAA and lower co-array redundancy. Comparisons and simulation results verified the superiority of the proposed ENAFS for DOA estimation of NC signals.

References

[1] FRIEDLANDER B, WEISS A J. Direction finding in the presence of mutual coupling[J]. IEEE Transactions on Antennas and Propagation, 1991, 39(3): 273-284.

[2] SHI J, HU G, ZHANG X, et al. Sparsity-based DOA estimation of coherent and uncorrelated targets with flexible MIMO radar[J]. IEEE Transactions on Vehicular Technology, 2019, 68(6): 5835-5848.

[3] WANG X, WAN L, HUANG M, et al. Polarization channel estimation for circular and non-circular signals in massive MIMO systems[J]. IEEE Journal of Selected Topics in Signal Processing, 2019, 13(5): 1001-1016.

[4] WANG H, WAN L, DONG M, et al. Assistant vehicle localization based on three collaborative base stations via SBL-based robust DOA estimation[J]. IEEE Internet of Things Journal, 2019, 6(3): 5766-5777.

[5] FOCSHINI G J, GOLDEN G D, VALENZUELA R, et al. Simplified processing for high spectral efficiency wireless communication employing multi-element arrays[J]. IEEE Journal on Selected Areas on Communications, 1999, 17(11): 1841-1852.

[6] CONG L, ZHUANG W. Hybrid TDOA/AOA mobile user location for wideband CDMA cellular systems[J]. IEEE Transactions on Wireless Communications, 2002, 1(3): 439-447.

[7] WANG J, DING G, WU Q, et al. Spatial-temporal spectrum hole discovery: A hybrid spectrum sensing and geolocation database framework[J]. Chinese Science Bulletin, 2014, 59: 1896-1902.

[8] ZHANG X, XU D. Angle estimation in bistatic MIMO radar using improved reduced dimension Capon algorithm[J]. Journal of Systems Engineering and Electronics, 2013, 24(1): 84-89.

[9] YUE H, ZHANG X. Harmonic and interharmonic frequency estimation for power systems via segmented coprime sampling[J]. Transactions of Nanjing University of Aeronautics and Astronautics, 2023, 40(1): 71-79.

[10] SCHMIDT R. Multiple emitter location and signal parameter estimation[J]. IEEE Transactions on Anten-

nas and Propagation, 1986, 34(3): 276-280.

[11] ROY R, KAILATH T. ESPRIT-estimation of signal parameters via rotational invariance techniques[J]. IEEE Transactions on Acoustics, Speech, and Signal Processing, 1989, 37(7): 984-995.

[12] VAIDYANATHAN P P, PAL P. Sparse sensing with co-prime samplers and arrays[J]. IEEE Transactions on Signal Processing, 2010, 59(2): 573-586.

[13] PAL P, VAIDYANATHAN P P. Nested arrays: A novel approach to array processing with enhanced degrees of freedom[J]. IEEE Transactions on Signal Processing, 2010, 58(8): 4167-4181.

[14] MOFFET A. Minimum-redundancy linear arrays[J]. IEEE Transactions on Antennas and Propagation, 1968, 16(2): 172-175.

[15] WANG W, REN S, CHEN Z. Unified coprime array with multi-period subarrays for direction-of-arrival estimation[J]. Digital Signal Processing, 2018, 74: 30-42.

[16] WANG X, WANG X. Hole identification and filling in *K*-times extended co-prime arrays for highly efficient DOA estimation[J]. IEEE Transactions on Signal Processing, 2019, 67(10): 2693-2706.

[17] LIU J, ZHANG Y, LU Y, et al. Augmented nested arrays with enhanced DOF and reduced mutual coupling[J]. IEEE Transactions on Signal Processing, 2017, 65(21): 5549-5563.

[18] PAL P, VAIDYANATHAN P P. Coprime sampling and the MUSIC algorithm[C]//Proceedings of 2011 Digital signal processing and signal processing education meeting (DSP/SPE). Sedona, AZ, USA: IEEE, 2011: 289-294.

[19] MOGHADAM G S, SHIRAZI A A B. DOA estimation with extended optimum co-prime sensor array (EOCSA)[C]//Proceedings of 2019 Sixth Iranian Conference on Radar and Surveillance Systems. Isfahan, Iran: IEEE, 2019: 1-6.

[20] RAZA A, LIU W, SHEN Q. Thinned coprime array for second-order difference co-array generation with reduced mutual coupling[J]. IEEE Transactions on Signal Processing, 2019, 67(8): 2052-2065.

[21] LIU C L, VAIDYANATHAN P P. Super nested arrays: Linear sparse arrays with reduced mutual coupling—Part I: Fundamentals[J]. IEEE Transactions on Signal Processing, 2016, 64(15): 3997-4012.

[22] SHI J, HU G, ZHANG X, et al. Generalized nested array: Optimization for degrees of freedom and mutual coupling[J]. IEEE Communications Letters, 2018, 22(6): 1208-1211.

[23] LIU J, ZHANG Y, LU Y, et al. Augmented nested arrays with enhanced DOF and reduced mutual coupling[J]. IEEE Transactions on Signal Processing, 2017, 65(21): 5549-5563.

[24] QIN S, ZHANG Y D, AMIN M G. Generalized coprime array configurations for direction-of-arrival estimation[J]. IEEE Transactions on Signal Processing, 2015, 63(6): 1377-1390.

[25] LAI X, ZHANG X, HAN S, et al. Multi-layer filled coprime arrays for DOA estimation with extended hole-free coarray[J]. IEEE Transactions on Vehicular Technology, 2023, 73(2): 2621-2632.

[26] CHEN Z, DING Y, REN S, et al. A novel noncircular MUSIC algorithm based on the concept of the difference and sum coarray[J]. Sensors, 2018, 18(2): 344.

[27] GUPTA P, AGRAWAL M. Design and analysis of the sparse array for DOA estimation of noncircular signals[J]. IEEE Transactions on Signal Processing, 2018, 67(2): 460-473.

[28] LIN X P, ZHOU M J, ZHANG X F, et al. Computationally efficient direction of arrival estimation for improved nested linear array[J]. Transactions of Nanjing University of Aeronautics and Astronautics, 2019, 36(6): 1018-1025.

[29] MA W K, HSIEH T H, CHI C Y. DOA estimation of quasi-stationary signals with less sensors than sources and unknown spatial noise covariance: A Khatri-Rao subspace approach[J]. IEEE Transactions on Signal Processing, 2009, 58(4): 2168-2180.

[30] ABEIDA H, DELMAS J P. MUSIC-like estimation of direction of arrival for noncircular sources[J]. IEEE Transactions on Signal Processing, 2006, 54(7): 2678-2690.

[31] ZHANG X, XU L, XU L, et al. Direction of departure (DOD) and direction of arrival (DOA) estimation in MIMO radar with reduced-dimension MUSIC[J]. IEEE Communications Letters, 2010, 14(12): 1161-1163.

[32] ZHENG W, ZHANG X, WANG Y, et al. Padded coprime arrays for improved DOA estimation: Exploiting hole representation and filling strategies[J]. IEEE Transactions on Signal Processing, 2020, 68: 4597-4611.

[33] SVANTESSON T. Modeling and estimation of mutual coupling in a uniform linear array of dipoles[C]//Proceedings of 1999 IEEE International Conference on Acoustics, Speech, and Signal Processing. Phoenix, AZ,USA: IEEE, 1999, 5: 2961-2964.

[34] FRIEDLANDER B, WEISS A J. Direction finding in

the presence of mutual coupling[J]. IEEE Transactions on Antennas and Propagation, 1991, 39(3): 273-284.

Acknowledgements This work was supported by China National Science Foundations (Nos.62371225, 62371227).

Authors

The first author Mr. **LI Xiaolong** received the B.E. degree from Nanjing University of Aeronautics and Astronautics, Nanjing, China, in 2023, where he is currently pursuing the M.S. degree in College of Electronic and Information Engineering. His research interests include array signal processing and communication signal processing.

The corresponding author Prof. **ZHANG Xiaofei** received the M.S. degree in electrical engineering from Wuhan University, Wuhan, China, in 2001, and the Ph.D. degree in communication and information systems from Nanjing University of Aeronautics and Astronautics, Nanjing, China, in 2005. He is currently a professor with College of Electronic and Information Engineering, Nanjing University of Aeronautics and Astronautics. His research interests include array signal processing, communication signal processing, and multidimension systems.

Author contributions Mr. **LI Xiaolong** proposed the idea, wrote the manuscript, completed the simulations and conducted the analysis. Prof. **ZHANG Xiaofei** designed the structure of manuscript and guided the simulations. Mr. **SHEN Zihan** contributed to the discussion and background of the study. All authors commented on the manuscript draft and approved the submission.

Competing interests The authors declare no competing interests.

(Production Editor: ZHANG Huangqun)

用于非圆信号DOA估计的扩展填充嵌套阵列

李晓龙[1,2], 张小飞[1,2], 申子晗[1,2]

(1.南京航空航天大学电子信息工程学院,南京 211106,中国; 2.南京航空航天大学电磁频谱空间认知动态系统工业和信息化部重点实验室,南京 211106,中国)

摘要:稀疏阵列设计对于提高非圆(Non-circular, NC)信号的到达方向(Direction of arrival,DOA)估计精度具有重要意义。本文提出了一种基于孔洞填充策略的带填充传感器的扩展嵌套阵列(Extended nested array with a filled sensor, ENAFS)。首先介绍了改进的嵌套阵列(Improved nested array, INA)结构并证明了它的性质。随后,通过添加额外的传感器来填充孔洞,扩展了和差共阵列(Sum-difference coarray, SDCA),因此获得了更大的均匀自由度(uniform Degree of freedom, uDOF)和虚拟阵列孔径(Virtual array aperture, VAA),从而设计了ENAFS结构。最后,仿真结果验证了所提出的阵列结构在自由度、互耦和DOA估计性能方面的优越性。

关键词:非圆信号;扩展嵌套阵列;稀疏阵列;到达方向估计;和差共阵列